Size Distribution of Linear and Helical Polymers in Actin Solution Analyzed by Photon Counting Histogram

Naofumi Terada,* Togo Shimozawa,† Shin'ichi Ishiwata,*†‡ and Takashi Funatsu§¶

*Integrated Bioscience and Biomedical Engineering, Graduate School of Science and Engineering, †Department of Physics, Faculty of Science and Engineering, and ‡Advanced Research Institute for Science and Engineering, Waseda University, Shinjuku-ku, Tokyo, Japan; §Graduate School of Pharmaceutical Sciences, The University of Tokyo, Bunkyo-ku, Tokyo, Japan; and ¶Core Research for Evolutional Science and Technology, Japan Science and Technology Agency, Saitama, Japan

ABSTRACT Actin is a ubiquitous protein that is a major component of the cytoskeleton, playing an important role in muscle contraction and cell motility. At steady state, actin monomers and filaments (F-actin) coexist, and actin subunits continuously attach and detach at the filament ends. However, the size distribution of actin oligomers in F-actin solution has never been clarified. In this study, we investigated the size distribution of actin oligomers using photon-counting histograms. For this purpose, actin was labeled with a fluorescent dye, and the emitted photons were detected by confocal optics (the detection volume was of femtoliter (fL) order). Photon-counting histograms were analyzed to obtain the number distribution of actin oligomers in the detection area from their brightness, assuming that the brightness of an oligomer was proportional to the number of protomers. We found that the major populations at physiological ionic strength were 1–5mers. For data analysis, we successfully applied the theory of linear and helical aggregations of macromolecules. The model postulates three states of actin, i.e., monomers, linear polymers, and helical polymers. Here we obtained three parameters: the equilibrium constants for polymerization of linear polymers, $K_l = (5.2 \pm 1.1) \times 10^6\ M^{-1}$, and helical polymers, $K_h = (1.6 \pm 0.5) \times 10^7\ M^{-1}$; and the ratio of helical to linear trimers, $\gamma = (3.6 \pm 2.3) \times 10^{-2}$. The excess free energy of transforming a linear trimer to a helical trimer, which is assumed to be a nucleus for helical polymers, was calculated to be 2.0 kcal/mol. These analyses demonstrate that the oligomeric phase at steady state is predominantly composed of linear 1–5mers, and the transition from linear to helical polymers occurs on the level of 5–7mers.

INTRODUCTION

Actin is a ubiquitous protein, whose polymerization-depolymerization dynamics plays an important role in cell motility. At low-salt conditions, actin exists as monomers (G-actin), but polymerizes, forming filaments (F-actin), at physiological ionic conditions, if the concentration of actin monomers exceeds the critical concentration for polymerization (1). Actin polymerization starts after the polymerization nucleus is formed, and the polymerization rate depends on the total concentration of actin. Until now, actin polymerization has been studied by measuring viscosity (1), by static (2) and dynamic (3) light-scattering of the solution, by monitoring changes in fluorescence intensity of pyrenyl iodoacetamide-labeled actin (2), and so on. At steady state, actin monomers and filaments coexist, and monomers continue to attach and detach at the ends of filaments. Electron microscopy was used to study the distribution of the lengths of F-actin (4,5), to determine the asymmetrical growth rates at both ends of F-actin (6,7), and to observe direct coupling of short fragments of F-actin (7,8). Fluorescence microscopy observation of F-actin labeled with rhodamine-phalloidin allowed measurement of filament lengths and flexibility (9,10). Recently, polymerization dynamics of individual F-actin filaments was visualized by total internal reflection fluorescence microscopy (11–14), and large length fluctuations of the filaments provoked speculations that growth may proceed by oligomeric, in addition to monomeric, association-dissociation events (13). This inspired us to study the size distribution of actin oligomers at physiological ionic conditions.

The length distribution of F-actin polymerized in vitro was initially investigated by electron microscopy (4,5) and later by fluorescence microscopy (15). These studies reported the exponential distribution of F-actin particle lengths, supporting the theory of linear and helical aggregates (1,16). In this theory, the equilibrium between monomers and linear polymers, and between monomers and helical filaments, is postulated. Nucleation involves the association of three to four monomers into a stable nucleus from which a filament elongates by stochastic association of monomers to the ends of filaments. Filament elongation continues until the equilibrium phase, or steady state, is reached, where the rates of monomer association and dissociation are precisely balanced. In this phase, the stochastic exchange of monomers between filaments of different lengths leads to the redistribution of filament lengths, resulting in exponential distribution of lengths. To check the validity of this theory, the size distribution of small oligomers (1–10mers) has to be determined experimentally; however, it was impossible to do this by conventional methods.

To overcome this obstacle, we measured the size distribution of actin oligomers using the photon-counting histogram

Submitted October 5, 2006, and accepted for publication November 22, 2006.

Address reprint requests to Takashi Funatsu, Laboratory of Bio-Analytical Chemistry, Graduate School of Pharmaceutical Sciences, The University of Tokyo, 7-3-1, Hongo, Bunkyo-ku, Tokyo 113-0033, Japan. Tel.: 81-3-5841-4760; Fax: 81-3-5802-3339; E-mail: funatsu@mail.ecc.u-tokyo.ac.jp.

0006-3495/07/03/2162/10 $2.00

doi: 10.1529/biophysj.106.098871

(PCH) technique (17). This method enabled us to determine two parameters for each fluorescent species present, namely, the average number and brightness of the fluorescent particles in the observation volume, which in turn allowed us to distinguish between different species based on the difference in brightness. This method has been successfully applied to confirm protein oligomerization in living cells (18) and interactions between oligonucleotides and polycationic polymers (19). Recently, PCH analysis was extended to one-photon excitation for confocal spectroscopy (20–22). Here we use this PCH analysis to study the number distribution of actin oligomers. For this purpose, Cys-374 of actin was labeled with BODIPY FL-iodoacetamide, since labeling with this dye does not affect the polymerization-depolymerization dynamics of actin, as confirmed in the study described here. In addition, there exists a wavelength range in which the fluorescence intensity does not change upon polymerization, which is a requirement for PCH analysis. Photons emitted from the labeled actin were detected by confocal optics, and PCHs were analyzed to determine the size distribution of actin oligomers. Finally, the data were successfully analyzed by applying the theory of linear and helical aggregation of macromolecules (1,16).

MATERIALS AND METHODS

Preparation of fluorescent actin

G-actin was purified from acetone powder of rabbit skeletal muscle according to Spudich and Watt (23), except that the tropomyosin-troponin complex was removed before the preparation of the acetone powder, as previously described (7). G-actin was solubilized in 2 mM Tris-HCl (pH 8.0), 50 μM $CaCl_2$, 0.1 mM ATP, and 2 mM sodium azide. The concentration of unlabeled actin was determined from ultraviolet absorption (V-550, JASCO, Tokyo, Japan), assuming the molar extinction coefficient at 290 nm, 26,600 M^{-1} cm^{-1} (24). Labeling with fluorescent dye was performed by incubating 48 μM F-actin in a solution containing 0.1 M KCl, 2 mM $MgCl_2$, 1 mM ATP, 2 mM Tris-HCl (pH 8.0), and 200 μM *N*-((4,4-difluoro-5,7-dimethyl-4-bora-3a,4a-diaza-s-indacene-3-yl)methyl)iodoacetamide (BODIPY FL C_1-IA) (D6003, Molecular Probes, Eugene, OR) for 2 h at room temperature. BODIPY FL C_1-IA dissolved in dimethylformamide (20 mM) was slowly added to actin solution with continuous stirring. The reaction was terminated by adding 5 mM dithiothreitol (DTT), and BODIPY FL-labeled actin was centrifuged at 411,000 $\times$ *g* for 45 min at 8°C. The pellet was then dissolved in and dialyzed against a solution containing 20 mM MOPS (pH 7.0), 50 μM $CaCl_2$, 0.1 mM ATP, 1 mM DTT, and 1 mM sodium azide for 24 h at 2°C. After centrifugation at 411,000 $\times$ *g* for 20 min at 2°C, free fluorescent dye was removed from the G-actin solution by Sephadex G25 column chromatography. The concentration of BODIPY FL was estimated from the molar extinction coefficient at 505 nm, 49,000 M^{-1} cm^{-1}. The concentration of labeled actin was determined by subtracting 0.029 $\times$ A_{505} from the A_{290} value. The molar ratio of dye to actin in solution was 96–105% throughout the study. Pyrene iodoacetamide-labeled actin (P29, Molecular Probes) was prepared similarly, and the average labeling ratio was 105%.

Fluorescence spectroscopy of pyrene-actin and BODIPY FL-actin

To evaluate the effect of BODIPY FL labeling on polymerization of actin, pyrene-actin and BODIPY FL-actin of various mixing ratios were copolymerized, and the fluorescence intensity of pyrene was measured as follows (Fig. 1) 0.5 μM pyrene-actin and 0–4.5 μM BODIPY FL-actin were mixed with unlabeled actin so as to keep the total concentration of actin at 5 μM in buffer G (20 mM MOPS (pH 7.0), 50 μM $CaCl_2$, 1 mM ATP, and 1 mM DTT) containing 0.1 mg/ml BSA. To change actin-bound cations from Ca^{2+} to Mg^{2+}, 1/20 volume of mixed solution of 1 mM $MgCl_2$ and 4 mM EGTA was added to actin solution 5 min before the initiation of the polymerization at 27°C. Actin was polymerized by adding 1/20 volume of mixed solution of 1 M KCl and 40 mM $MgCl_2$. The time course of the fluorescence intensity of pyrene was measured at 27°C using a fluorescence spectrometer (F-4500, Hitachi, Tokyo, Japan) with excitation wavelength of 365 nm and emission wavelength of 408 nm.

Next, changes in the fluorescence spectra of BODIPY FL-actin upon polymerization were monitored as follows (Fig. 2). The polymerization of BODIPY FL-actin (5 μM) in buffer G was initiated by adding 1/20 volume of mixed solution of 2 M KCl and 40 mM $MgCl_2$, and fluorescence spectra were measured using the fluorescence spectrometer with excitation wavelength of 488 nm. The scan time of each spectrum was 3 s.

The dependence of the fluorescence intensity of BODIPY FL-actin on the labeling ratio was measured as follows (Fig. 3). BODIPY FL-actin was mixed with unlabeled actin in buffer G at various ratios such that the proportion of BODIPY FL-actin was 5–100% and the total concentration of actin was kept at 500 nM. Then actin was polymerized by adding 1/20 volume of mixed solution of 2 M KCl and 40 mM $MgCl_2$ and incubated overnight at room temperature. Fluorescence intensity was measured using the fluorescence spectrometer with excitation wavelength of 488 nm and emission wavelength of 507 nm.

Instrumentation and data analysis of PCH

The photon counting experiments were carried out using an inverted microscope with a 60$\times$ water immersion objective (UPlanApo, 60$\times$w, NA 1.2, Olympus, Tokyo, Japan). Light from a solid-state laser (488 nm, Sapphire 488-20, Coherent, Tokyo, Japan) was reflected by a dichroic mirror (485DRLP, Omega Optical, Brattleboro, VT), and focused using the objective. The power of the laser was 13 μW at the focal plane. The fluorescence from the sample was collected by the objective, passed through the dichroic mirror, emission filters (D520/40m and S500/22m, Chroma

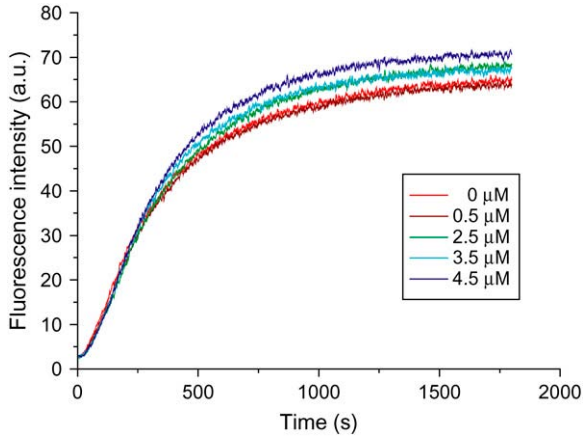

FIGURE 1 Time course of the fluorescence intensity of pyrene-actin copolymerized with various mixing ratios of BODIPY FL-actin. The concentration of pyrene-actin was 0.5 μM, and the concentrations of BODIPY FL-actin were varied from 0 to 4.5 μM. Total concentration was kept at 5 μM by adding unlabeled actin. Polymerization of actin was initiated by the addition of 50 mM KCl and 2 mM $MgCl_2$ to buffer G at 27°C. The polymerization rates were similar irrespective of the mixing ratios of BODIPY FL-actin, although the fluorescence intensity of pyrene was ~10% higher in 4.5 μM BODIPY FL-actin than in actin not labeled with BODIPY FL.

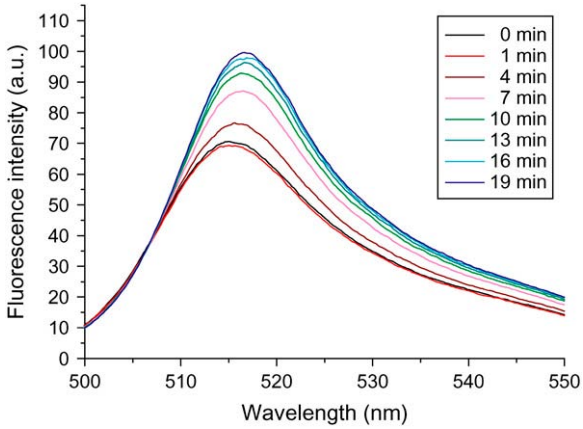

FIGURE 2 Time course of the fluorescence spectrum of BODIPY FL (~100% labeled)-actin after initiation of polymerization. Polymerization of BODIPY FL-actin was initiated by the addition of 0.1 M KCl and 2 mM $MgCl_2$ to buffer G at 27°C, and the fluorescence spectra of BODIPY FL were measured at each time point indicated in the graph. The spectrum at 0 min shows the spectrum in buffer G before the addition of KCl and $MgCl_2$.

Technology, Bellows Falls, VT), and a pinhole (diameter, 30 μm) located at the position conjugated to the focal plane. The transmission wavelength of the emission filters was from 502 to 512 nm. The fluorescence that passed through the pinhole was introduced into an optical fiber coupled to an avalanche photodiode (SPCM-AQR-14-PC, PerkinElmer, Wellesley, MA). The output of the avalanche photodiode was put into a counter (C8855, Hamamatsu Photonics, Hamamatsu City, Japan) with a gate time of 100 μs. A photon counting histogram was obtained from the data collected over a period of 100 s. Fitting of the data was performed according to the method of Chen et al. (17), using the correction for one-photon excitation (20). The correction parameter, F, for BODIPY FL was determined to be 0.70 ± 0.35 (mean ± SD, $n = 16$) (20,22). The program for the fitting was built with numerical routines according to Press and co-workers (25) by Visual C++ software (Microsoft, Redmond, WA).

PCH measurement

G-actin was diluted to 300 nM, 500 nM, 700 nM, and 1 μM with buffer G and incubated overnight at 0°C. F-actin was prepared by incubating actin at the above concentrations in buffer F (0.1 M KCl, 2 mM $MgCl_2$, 20 mM MOPS (pH 7.0), 50 μM $CaCl_2$, 1 mM ATP, and 1 mM DTT) overnight at room temperature. A 50-μl portion of each actin solution was placed on a coverslip, and the focal plane of the microscope was adjusted at 30 μm from the glass/solution interface. All PCH measurements were done at 23°C. PCHs of BODIPY FL-actin in buffer G were analyzed as follows.

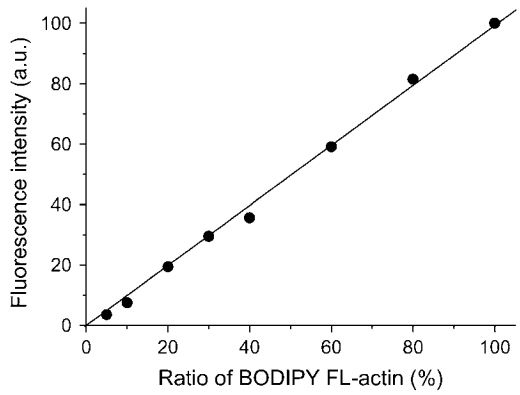

FIGURE 3 Fluorescence intensity versus a mixing ratio of BODIPY FL-actin. Actin containing various ratios of BODIPY FL-actin was polymerized in buffer F overnight at room temperature. Fluorescence intensity of F-actin solution was proportional to the labeling ratio of BODIPY FL-actin. The data were fit by a straight line.

The PCH for identical but independent particles is determined by two parameters, namely, N, the average number of molecules within the observation volume, and ε, the detected photon counts/molecule/sampling time. The probability of detecting k photoelectrons per sampling time is

$$\Pi(k;N,\varepsilon)=\sum_{M=0}^{\infty}p^{(M)}(k;V_0,\varepsilon)\frac{N^M e^{-N}}{M!}, \tag{1}$$

where V_0 is the reference volume. $p^{(M)}(k;V_0,\varepsilon)$ is the probability of detecting k photon counts from M fluorescent particles, defined as follows:

$$p^{(0)}(k;V_0,\varepsilon)=\begin{cases}1, \text{ for } k=0\\ 0, \text{ for } k\geq 1\end{cases} \tag{2}$$

$$p^{(1)}(k;V_0,\varepsilon)=\begin{cases}\dfrac{1}{(1+F)^2}\dfrac{1}{V_0}\dfrac{\pi\omega_0^2 z_0}{k!}\displaystyle\int_0^{\infty}\Gamma(k,\varepsilon e^{-2x^2})dx \\ \quad+\dfrac{\pi^{3/2}\omega_0^2 z_0}{V_0(1+F)^2}\dfrac{1}{2\sqrt{2}}\varepsilon, & \text{for } k=1\\ \dfrac{1}{(1+F)^2}\dfrac{1}{V_0}\dfrac{\pi\omega_0^2 z_0}{k!}\displaystyle\int_0^{\infty}\Gamma(k,\varepsilon e^{-2x^2})dx, & \text{for } k>1\end{cases} \tag{3}$$

where ω_0 is the beam waist and z_0 is the effective length of the confocal volume, Γ is the incomplete gamma function, and F is the correction parameter for one-photon excitation (21).

The M-particle PCH $p^{(M)}(k;V_0,\varepsilon)$was constructed by convolution of multiple single-particle PCHs $p^{(1)}(k;V_0,\varepsilon)$, as follows:

$$p^{(M)}(k;V_0,\varepsilon)=\underbrace{(p^{(1)}\otimes\cdots\otimes p^{(1)})}_{M\text{ times}}(k;V_0,\varepsilon). \tag{4}$$

If n different but independent particles (1, …, n) are present, the PCH is obtained by convoluting the PCHs of individual species (17), as shown in Eq. (5):

$$\Pi(k;N_1,\cdots,N_n,\varepsilon_1,\cdots,\varepsilon_n)=\Pi(k;N_1,\varepsilon_1)\otimes\cdots\otimes\Pi(k;N_n,\varepsilon_n). \tag{5}$$

To fit the data, the histogram of the experimental data was calculated and then normalized to yield the experimental photon counting probability density $p(k)$. Since the probability of detecting k counts of photoelectrons for r times out of M trials (10^6 in our experiments) is given by the binominal distribution function, the expectation value is represented by $\langle r\rangle = Mp(k)$, and the standard deviation by $\sigma=[Mp(k)(1-p(k))]^{1/2}$. To obtain the best-fit parameters of N_i and ε_i ($1\leq i\leq n$), the theoretical density function was calculated for all the combinations of these parameters, and the combination of parameters N_i and ε_i that minimizes the following χ^2 function (17) was adopted as the best fit.

$$\chi^2=\frac{\displaystyle\sum_{k=k_{min}}^{k_{max}}\left(M\frac{p(k)-\Pi(k;N_1,\cdots,N_n,\varepsilon_1,\cdots,\varepsilon_n)}{\sigma}\right)^2}{k_{max}-k_{min}-2n}. \tag{6}$$

To analyze the number distribution of oligomers in buffer G, we assumed the number of species of actin oligomers, n, in buffer G to be distributed between 1 and 5 and fitted the data with the theoretical density functions $\Pi(k;N,\varepsilon)$, $\Pi(k;N_1,N_2,\varepsilon_1,\varepsilon_2)$, …, $\Pi(k;N_1,\cdots N_5,\varepsilon_1,\cdots\varepsilon_5)$ by changing N_i

and ε_i as parameters. Then we determined n so as to minimize the χ^2 function (Eq. 6). Similar analyses were performed assuming that the number of species of actin oligomers in buffer F is distributed between 1 and 9.

We determined the number of protomers in each oligomer from the brightness, ε_i, assuming that the brightness of i-mers was i times that of the monomer. The number distribution of actin oligomers was obtained from N_i, the average number of oligomers within the observation volume. Finally, we calculated the proportion of the oligomers in total number concentration.

RESULTS

Polymerizability of BODIPY FL-actin

Labeling of Cys-374 with rhodamine-maleimide was reported to decrease the elongation rate of actin (11). To study the size distribution of F-actin by PCH, actin must be labeled with a fluorescent dye that does not affect the polymerization-depolymerization dynamics. We found that BODIPY FL iodoacetamide fulfilled this requirement. The polymerization of actin containing various ratios of BODIPY FL-labeled actin was initiated by the addition of 50 mM KCl and 2 mM $MgCl_2$. Pyrene-labeled actin (0.5 μM) was also included to monitor the polymerization process by changes in its fluorescence intensity (2). The total concentration of actin was kept at 5 μM, because the time course of polymerization depends on actin concentration. As shown in Fig. 1, though the fluorescence intensity of pyrene in the presence of 90% BODIPY FL-labeled actin was ~10% higher than that of unlabeled actin, the polymerization rates were similar irrespective of the mixing ratio of BODIPY FL-actin. These results indicate that the labeling of actin by BODIPY FL does not affect its polymerizability.

Fluorescence spectrum of BODIPY FL-actin before and after the polymerization

To obtain information about the size of actin oligomers by PCH, the fluorescence intensity of BODIPY FL must be constant irrespective of whether actin is monomeric or filamentous, because the number of protomers in each oligomer is determined by assuming that its brightness is proportional to the number of protomers. The changes in the fluorescence spectra during polymerization of 100% labeled BODIPY FL-actin are shown in Fig. 2. The wavelength of the peak was red-shifted and the peak intensity increased by ~50% upon polymerization. However, the fluorescence intensity of BODIPY FL-actin between 500 and 510 nm hardly changed upon polymerization. Therefore, we looked for commercially available optical filters that transmitted in this range, and found that the combination of bandpass filters D520/40m and S500/22m gave suitable transmission in the 502–512 nm range. The change in the fluorescence intensity upon polymerization of BODIPY FL-actin in this range was <11%.

Fluorescence intensity of BODIPY FL-actin was proportional to labeling ratio

When two fluorescent molecules come very close to each other, quenching of fluorescence sometimes occurs. There remains concern that Cys-374 residues of the adjacent actin protomers are close enough to quench each other. If this were the case, it would be impossible to determine the size distribution of oligomers using PCH. To exclude this possibility, we examined the dependence of the fluorescence intensity of BODIPY FL-actin on the labeling ratio. In principle, the lower the labeling ratio, the longer the average distance between fluorescent molecules, so that lowering the labeling ratio should reduce the effect of quenching. If there are quenching effects, the fluorescence intensity must be saturated at a higher labeling ratio rather than being proportional to the labeling ratio. As shown in Fig. 3, we found that the fluorescence intensity was proportional to the labeling ratio of BODIPY FL-actin up to 100%, indicating that no quenching of BODIPY FL occurred in the PCH experiments.

PCHs of BODIPY FL-actin

When a BODIPY-FL actin species passed through the confocal volume of femtoliter order, bursts of photons were observed. Fig. 4 shows the typical time courses of photon counts from BODIPY FL-actin in buffer G (Fig. 4 *A*) and in buffer F (Fig. 4 *B*). The number of photons was counted every 100 μs, and one million data points were collected.

Typical PCHs of BODIPY FL-actin in buffer G are shown in Fig. 5, *A–D*. Briefly, they were analyzed as follows (see Materials and Methods for details). The PCHs were normalized

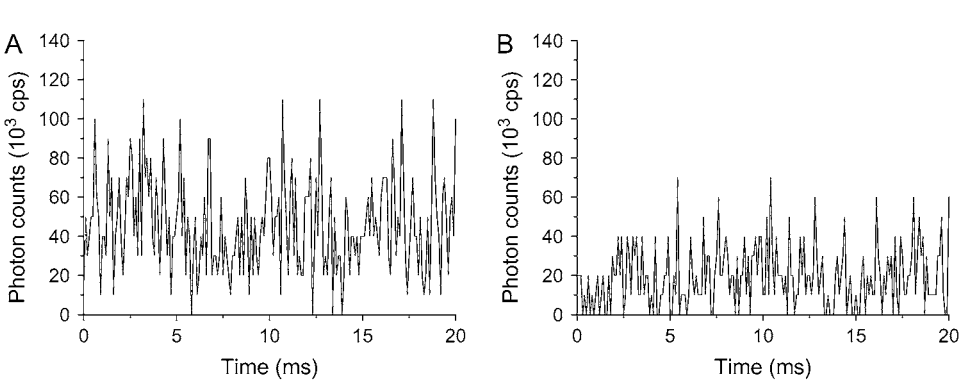

FIGURE 4 Time course of the fluorescence fluctuation profiles of 300 nM BODIPY FL-actin in buffer G (*A*) and buffer F (*B*) measured by the PCH setup.

to obtain the photon counting probability density, $p(k)$. We assumed that the number of species of actin oligomers, n, in buffer G was distributed between 1 and 5 and fitted the data with the theoretical density functions $\Pi(k; N, \varepsilon)$, $\Pi(k; N_1, N_2, \varepsilon_1, \varepsilon_2)$, $\cdots$, $\Pi(k; N_1, \cdots N_5, \varepsilon_1, \cdots \varepsilon_5)$ by changing N_i and ε_i as parameters. Then we determined n so as to minimize the χ^2 function (Eq. 6). Fig. 5 *E* shows the histogram of n obtained by 15 independent experiments at four different concentrations. The number of species of actin oligomers, n, was similar irrespective of the total actin concentration. About 90% of PCHs were fitted by the single component ($n = 1$) analysis and the remaining 10% were fitted by two components ($n = 2$). The reduced χ^2 function thus obtained was 1.1 ± 0.3 (mean $\pm$ SD). Next, we calculated the total number of protomers in each oligomer (see Fig. 7). The PCH analysis indicated that >99.5% of fluorescent actin in buffer G emitted photons at a similar rate ($(5.1 \pm 0.6) \times 10^3$ counts/s; mean $\pm$ SD, $n = 60$), suggesting that it was from monomeric BODIPY FL-actin. The content of oligomers (4–6mers) detected as the second component in Fig. 5 was <0.5%.

Next, we analyzed PCHs of BODIPY FL-actin in buffer F. Typical PCHs of BODIPY FL-actin in buffer F are shown in Fig. 6, *A–D*. We assumed that the number of species of actin oligomers, n, in buffer F was distributed from 1 to 9 and fitted the data as described above. Fig. 6 *E* shows the histogram of n obtained by 60 independent experiments at four different actin concentrations. The components larger than 100mers ($\sim$2%) were excluded from the analyses, because the length of such oligomers was greater than the width of the confocal volume. The components of less than one-half of the monomer brightness were also excluded from the analysis (the average brightness of such species was 1/7 of the monomer brightness). The number of species that minimized the χ^2 function was distributed between 2 and 8. The reduced χ^2 function thus obtained was 2.8 ± 2.0 (mean $\pm$ SD). Next, we calculated the total number of protomers in each oligomer assuming that the brightness of the monomer was 5.1×10^3 counts/s and that the brightness of an oligomer was proportional to the number of protomers. This assumption was justified by the observation that the major population in the

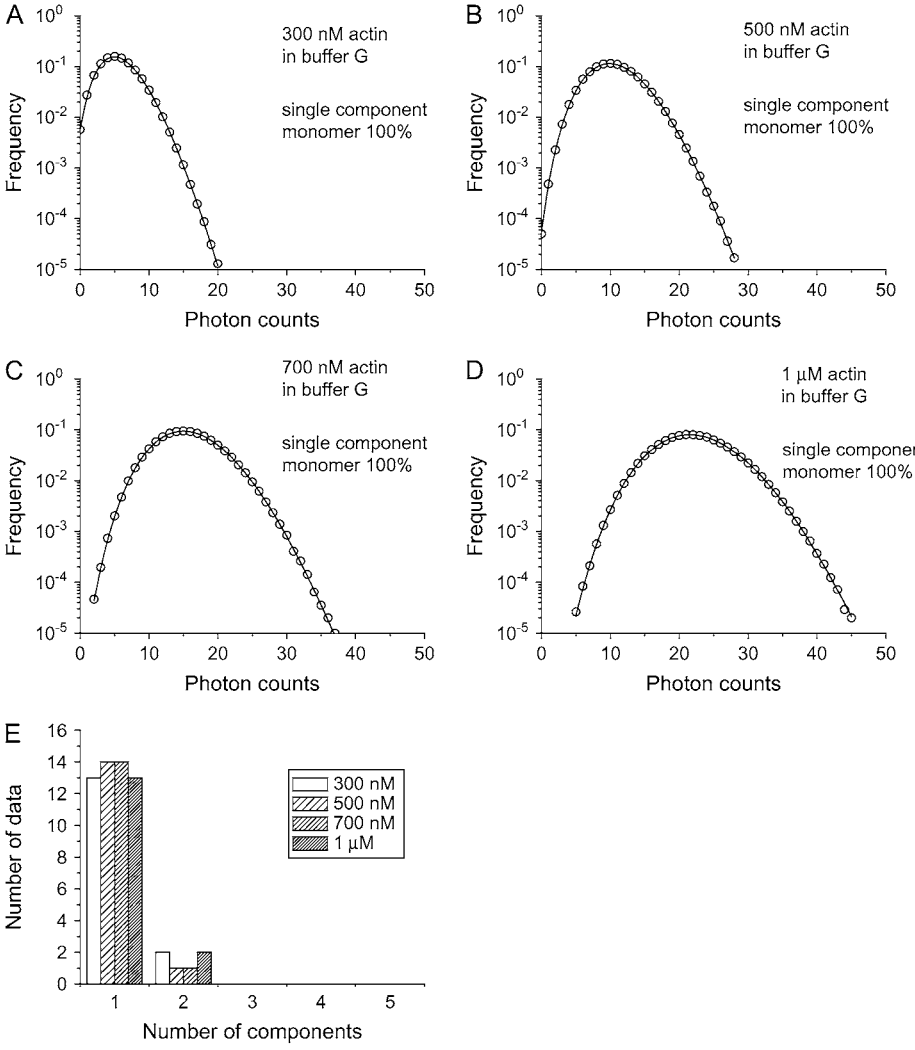

FIGURE 5 Examples of photon counting histograms of 300 nM (*A*), 500 nM (*B*), 700 nM (*C*), and 1 μM (*D*) BODIPY FL-actin in buffer G. The histograms are normalized to give the photon-counting probability density. The solid lines represent the best fit to the data. (*E*) The number of components required to fit the data. Most of the data could be fit assuming a single component (monomer). Panels *A–D* show the examples that could be fit by a single component, where the proportion of monomer was 100%.

brightness distribution of G-actin was at 5.1×10^3 counts/s and the histogram of brightness obtained by the PCH measurements in buffer F had peaks, or clusters, every 5×10^3 counts/s, namely, at $(5.6 \pm 1.2) \times 10^3$ counts/s, $(9.8 \pm 1.4) \times 10^3$ counts/s, and $(15.3 \pm 1.5) \times 10^3$ counts/s, corresponding to the brightness of a monomer, a dimer, and a trimer, respectively (see Supplementary Material).

Although the dimers, trimers, and oligomers were hardly detected in buffer G, they clearly existed in buffer F, as shown in Fig. 7. The major components of oligomers in buffer F were 1–5mers, and their total content was >94%. It should be noted that the distribution of oligomers could be classified into two populations having two different slopes for the relationship between the number concentration of *i*-mers and the value of *i* (Fig. 7). One class was 1–5mers and the other was 6–100mers. The two straight lines are crossed at around 6mer. The proportion of each oligomer larger than 6mer was <1%. The number concentrations of both populations were fitted by exponential functions with different parameters of *A* and *B* as follows:

$$c_i = A\exp(-Bi). \quad (7)$$

The obtained parameters of *A* and *B* are given in Table 1. The value of *B* is larger for 1–5mers than for 6–100mers, implying that the equilibrium constant of monomer and oligomer is lower for 1–5mers than for 6–100mers.

Based on the above analyses, we determined the number of actin monomers in both buffer G and buffer F in the confocal volume. As shown in Fig. 8, the number of actin monomers in buffer G linearly depends on actin concentration, whereas in buffer F it remains almost constant. It is to be noted, however, that the linear fit for the data in buffer G does not pass through the origin, which, at first glance, seems to indicate that the average number of monomers in the confocal volume was not exactly proportional to the total actin concentration. This result contradicts the observation that >99% of actin molecules were monomers in buffer G (Figs. 5 and 7). One plausible interpretation of this apparent discrepancy is that some part of actin molecules were adsorbed to the surface of a coverslip and the interface with

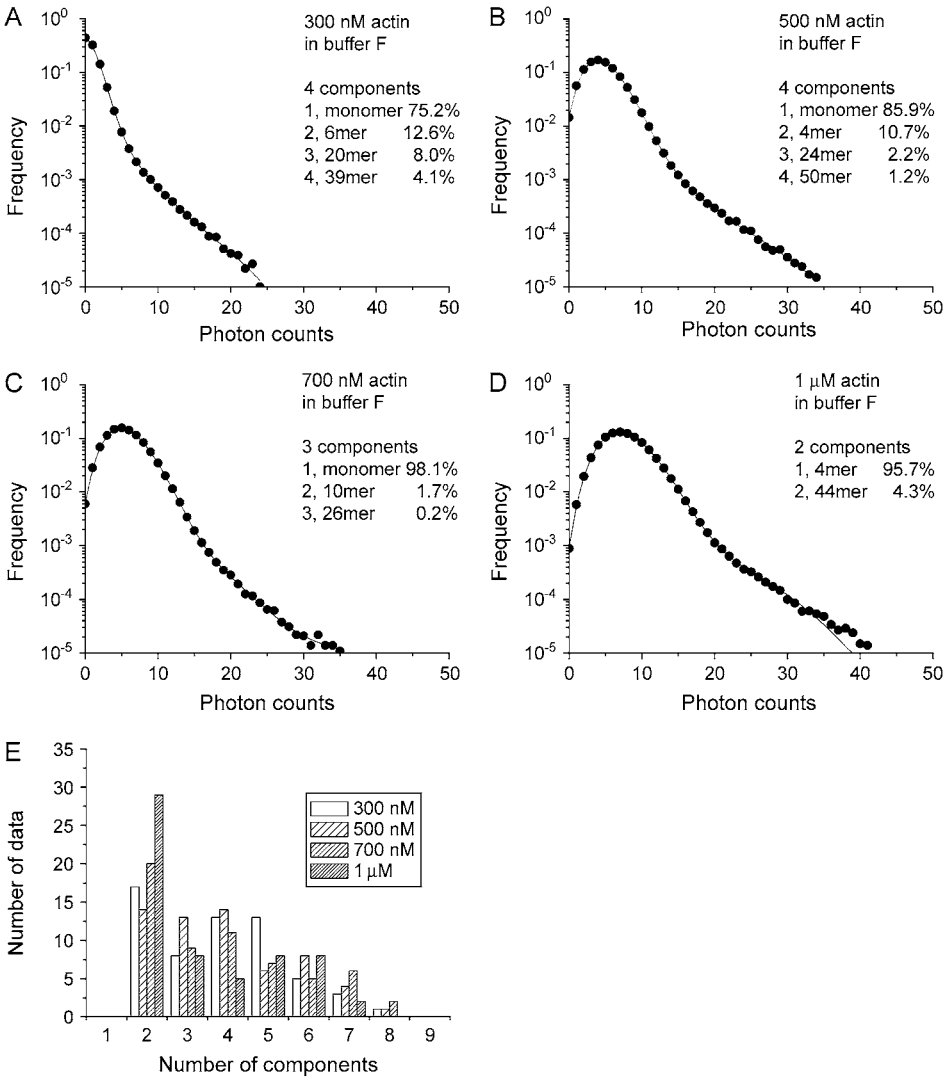

FIGURE 6 Examples of photon counting histograms of 300 nM (*A*), 500 nM (*B*), 700 nM (*C*), and 1 μM (D) BODIPY FL-actin in buffer F. The histograms are normalized to give the photon-counting probability density. The solid lines represent the best fit to the data. (*E*) The number of components required to fit the data was 2–8. Panels *A–D* show the examples that could be fit by three to four components. The proportions of the number concentration of each component are indicated in *A–D*.

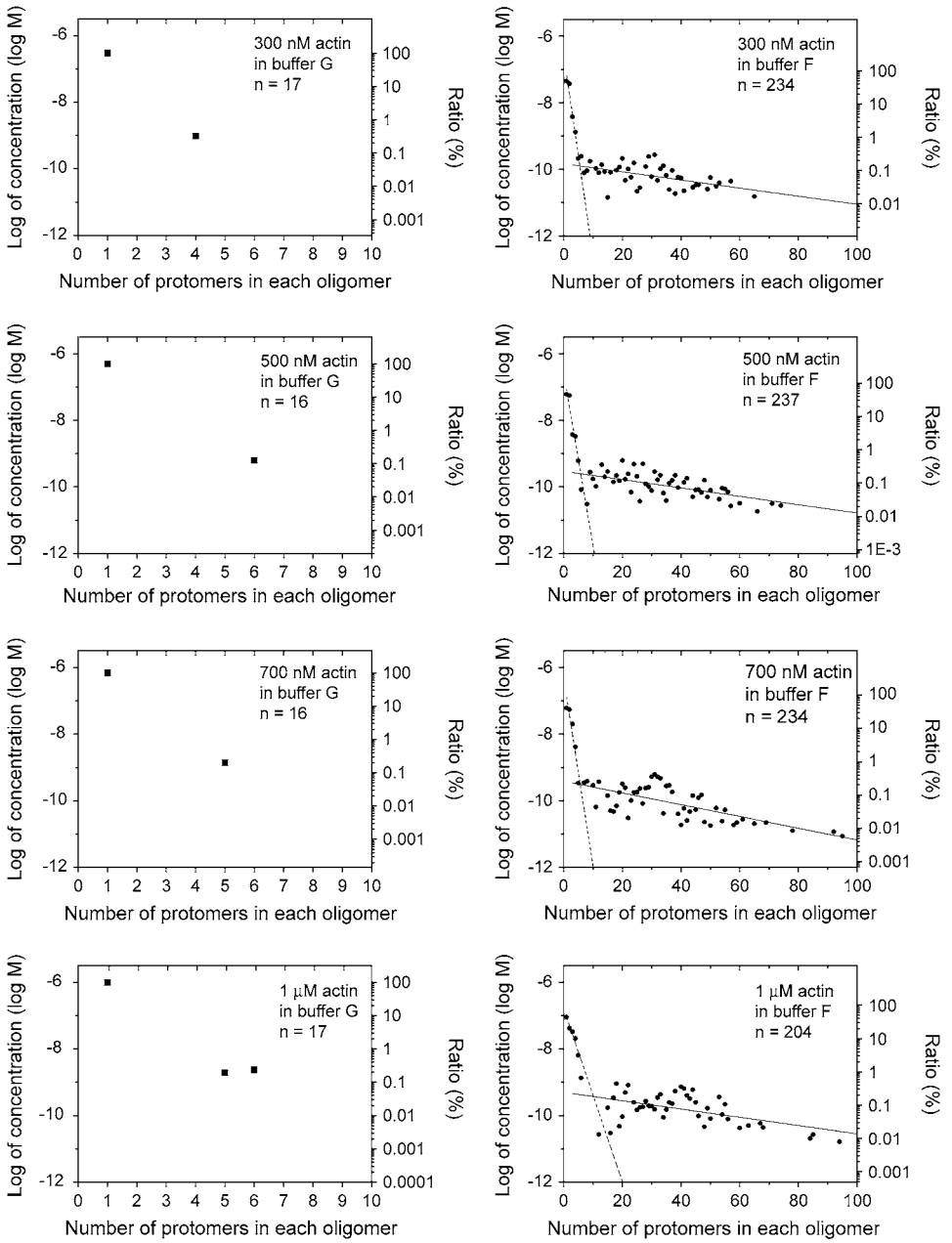

FIGURE 7 Logarithmic plot of the molar concentration of actin oligomers as a function of the number of protomers, *i*, in each oligomer. Most of the actin (>99%) in buffer G existed as monomers. The distribution of actin oligomers in buffer F had two distinct populations, 1–5mers and 6–100mers. The data for 1–5mers and 6–100mers were fit by dashed and solid lines, respectively.

air, so that the actual actin concentration was decreased by a fixed value proportional to the adsorption area. Based on this consideration, we set the cross-point of the linear fit with the abscissa as the true origin, implying that ~100 nM actin was adsorbed to the interface area of 50 μl of the actin solution used in the experiments. A rough estimation shows that the closely packed adsorption of actin molecules to the interface area is on the order of 10^{-11}–10^{-12} moles, which just corresponds to the loss of ~100 nM actin (= (10^{-11}–10^{-12} moles)/50 μl). On the other hand, the average number of monomers in the confocal volume in buffer F was 1.3 ± 0.4, irrespective of the total actin concentration. We consider that actin is adsorbed on the interface in buffer F in the same way, so that the newly determined origin is common for both conditions. Thus, the critical concentration for polymerization of actin in buffer F was determined to be 55 nM from the abscissa of the cross-point of the solid lines for buffer G and buffer F (Fig. 8).

DISCUSSION

PCH analysis to determine the size distribution of oligomers

So far, PCH analysis has been used to study the oligomerization of receptors in living cells (18). We have extended PCH analysis to probe much larger oligomers, i.e., actin polymers having an exponential length distribution at physiological

TABLE 1 Parameters for exponential fitting of the number concentration of *i*-mers

Conditions		*A* (M)*	*B**
300 nM	1–5mers	3.0×10^{-7}	1.4
	>5mers	1.5×10^{-10}	2.8×10^{-2}
500 nM	1–5mers	2.8×10^{-7}	1.2
	>5mers	2.9×10^{-10}	2.9×10^{-2}
700 nM	1–5mers	4.9×10^{-7}	1.3
	>5mers	3.9×10^{-10}	4.1×10^{-2}
1 μM	1–5mers	1.7×10^{-7}	6.0×10^{-1}
	>5mers	4.9×10^{-10}	2.9×10^{-2}

*The number concentration of *i*-mers, c_i, is fitted as $c_i = A\exp(-Bi)$.

ionic strength (buffer F). The analyses of PCH data showed that the oligomeric phase in steady state is predominantly composed of linear 1–5mers (Fig. 7). Because the proportion of oligomers larger than 6mers was <1%, the accumulation of a large amount of data had to be performed to confirm the exponential distribution of the number concentrations of longer oligomers. The obtained result is consistent with those of previous EM studies (4,5). The only difference from earlier EM results (4) is that our data show an eight-times-faster decrease in the number population from 6 to 100mers, which may be attributable to the differences in experimental conditions, such as protein concentration and solvent composition.

As observed in Fig. 7, the distribution of oligomers in buffer F has two markedly distinct regions, corresponding to 1–5mers and 6–100mers (cf. Table 1). The equilibrium constants of the monomer binding estimated from the slopes indicate that the constant of binding to 1–5mers is smaller than the constant of binding to 6–100mers. The most plausible interpretation is that the former corresponds to the monomer binding to linear oligomers, K_l, whereas the latter corresponds to binding to helical oligomers, K_h (for detailed analysis, see below). The crossing point of the two lines in the panels on the right in Fig. 7 suggests that the transition from linear to helical oligomers occurs at 5–7mers.

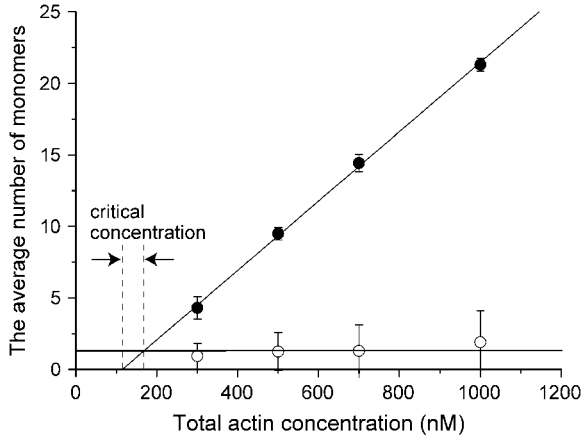

FIGURE 8 The average number of actin monomers within a confocal volume in buffer G (*solid circles*) and buffer F (*open circles*) as a function of total actin concentration. In buffer G, the number of monomers was proportional to the total actin concentration (*thin line*), but the fit did not pass through the origin. On the other hand, in buffer F, the number of monomers was almost constant. The critical concentration for polymerization was determined from the cross-point between the two lines (for details, see text). Error bars represent the standard deviation.

Analysis of PCH data by the theory of linear and helical aggregations of macromolecules

The PCH data obtained here were analyzed by the theory of Oosawa and Asakura, which postulates the equilibrium between monomers, linear polymers, and helical polymers, as shown in Fig. 9 *A* (1). The number concentrations of linear *i*-mers are denoted as c_{il}, which is given as follows:

$$c_{il} = K_l^{-1}(K_l c_1)^i, \tag{8}$$

where K_l is the equilibrium constant of monomer binding to a linear polymer, which is assumed to be independent of the degree of polymerization. The deformation of a linear polymer, leading to the creation of additional bonds, results in the formation of a helical polymer. Here we assume that the helical trimer is a nucleus for polymerization. Denoting the number concentration of helical *i*-mers as c_{ih},

$$c_{3h} = \gamma c_{3l} \tag{9}$$

and

$$c_{ih} = \gamma K_l^2 K_h^{-3}(K_h c_1)^i, \tag{10}$$

where γ is the concentration ratio of a helical to a linear trimer, and K_h is the equilibrium constant of monomer binding to the ends of the helical polymer. γ can be expressed by using the free energy ΔF necessary for the deformation of a linear trimer to produce a helical polymer as follows:

$$\gamma = \exp(-\Delta F/k_B T), \tag{11}$$

where k_B is the Boltzmann constant and T is absolute temperature.

The values of c_{ih} were obtained by logarithmic fitting of c_i in the panels on the right in Fig. 7 for $10 \le i < 100$ and extrapolating to $3 \le i < 10$. Accordingly, the values of c_{il} were obtained from $c_{il} = c_i$ (for $i = 1, 2$) and $c_{il} = c_i - c_{ih}$ (for $3 \le i < 10$). Then, the values of K_l, γ, and K_h were obtained from Eqs. 8–10, respectively. As a result, these three parameters were determined to be $K_l = (5.2 \pm 1.1) \times 10^6$ M^{-1}, $K_h = (1.6 \pm 0.5) \times 10^7$ M^{-1}, and $\gamma = (3.6 \pm 2.3) \times 10^{-2}$. A monomer attaches to two protomers at each end of a helical oligomer and to a single protomer in a linear oligomer, which results in the larger value of K_h compared to K_l. The critical concentration for polymerization was found to be $K_h^{-1} = 62$ nM, consistent with the value obtained from Fig. 8 (55 nM). The excess free energy of transforming a

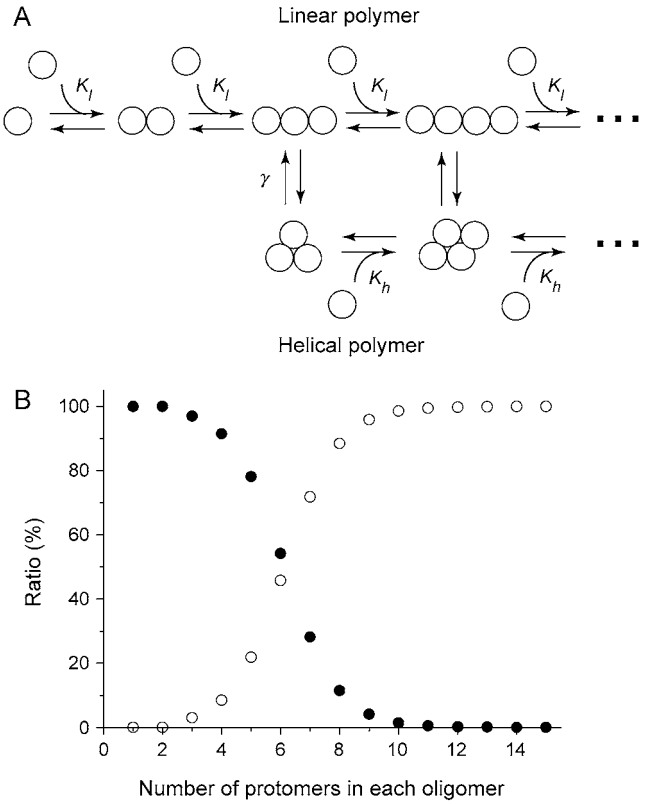

FIGURE 9 (*A*) Schematic diagram of the equilibrium of polymerization among monomers, linear polymers, and helical polymers used for the model analysis (for details, see Discussion). (*B*) Proportion of linear (*solid circles*) and helical (*open circles*) oligomers determined by Eqs. 8–10 and the data shown in Fig. 7. Here, the trimer was assumed to be the polymerization nucleus.

linear to a helical trimer, ΔF, was calculated to be 2.0 kcal/mol from Eq. 11.

Fig. 9 shows the existence ratio of linear and helical oligomers in 1–15mers determined from Eqs. 8–10 using the obtained values of the three parameters. These analyses suggest that 1), the oligomeric phase at steady state is predominantly composed of linear 1–5mers; 2), the transition from linear to helical oligomers occurs in 5–7mers (Fig. 9); and 3), most of the oligomers larger than 10mers are helical. In the analyses given above, we assumed that the helical trimer is a nucleus for polymerization. The analyses based on the assumption that the nucleus is the helical tetramer yielded a value of γ equal to $(1.3 \pm 1.1) \times 10^{-1}$ ($\Delta F = 1.2$ kcal/mol), whereas values of K_l and K_h remained unchanged, and the linear/helical existence ratio thus obtained was almost indistinguishable from that shown in Fig. 9 *B*. Therefore, from the present analyses, we cannot unambiguously deduce which oligomer serves as the polymerization nucleus. However, the trimer would be more probable due to the lower value of γ, which is the prerequisite for the condensation process of polymerization to helical assemblies such as actin filaments.

The most dominant species in the number distribution in F-actin solution is a monomer. Therefore, the most probable unit involved in polymerization events should be a monomer; however, the linear and helical oligomers identified in this study will also contribute to the polymerization dynamics of actin. In fact, our previous study indicated that the average size of a unit involved in the elementary process of polymerization-depolymerization dynamics is 5–6mers (13). Although structural studies on linear oligomers are necessary, future studies must also address the role of linear oligomers in polymerization dynamics.

CONCLUSIONS

The number distribution of actin oligomers in filamentous actin solution at physiological ionic conditions was determined using the PCH technique. The results confirm that the PCH is powerful enough to resolve the oligomeric state of fluorescently labeled actin. The experimental data were analyzed in terms of a theoretical model that assumes the equilibrium between monomers, linear and helical polymers of actin. This is the first report experimentally showing the existence of linear polymers in actin solution and indicating that the oligomeric phase at steady state is predominantly composed of linear 1–5mers. The transition from linear to helical polymers occurs on the level of 5–7mers.

We thank Dr. S. V. Mikhailenko for his critical reading of the manuscript.

This work was partly supported by Takeda Science Foundation and by Grants-in-Aid for Specially Promoted Research, Scientific Research (A), the 21st Century COE program, and ''Establishment of Consolidated Research Institute for Advanced Science and Medical Care'' from the Ministry of Education, Culture, Sports, Science and Technology (MEXT) of Japan.

REFERENCES

1. Oosawa, F., and S. Asakura. 1975. Thermodynamics of the polymerization of proteins. Academic Press, New York.
2. Kouyama, T., and K. Mihashi. 1981. Fluorimetry study of N-(1-pyrenyl)iodoacetamide-labelled F-actin. Local structural change of actin protomer both on polymerization and on binding of heavy meromyosin. *Eur. J. Biochem.* 114:33–38.
3. Masai, J., S. Ishiwata, and S. Fujime. 1986. Dynamic light-scattering study on polymerization process of muscle actin. *Biophys. Chem.* 25:253–269.
4. Kawamura, M., and K. Maruyama. 1970. Electron microscopic particle length of F-actin polymerized in vitro. *J. Biochem.* (*Tokyo*). 67:437–457.
5. Kawamura, M., and K. Maruyama. 1972. A further study of electron microscopic particle length of F-actin polymerized in vitro. *J. Biochem.* (*Tokyo*). 72:179–188.
6. Woodrum, D. T., S. A. Rich, and T. D. Pollard. 1975. Evidence for biased bidirectional polymerization of actin filaments using heavy meromyosin prepared by an improved method. *J. Cell Biol.* 67:231–237.
7. Kondo, H., and S. Ishiwata. 1976. Uni-directional growth of F-actin. *J. Biochem.* (*Tokyo*). 79:159–171.
8. Nakaoka, Y., and M. Kasai. 1969. Behaviour of sonicated actin polymers: adenosine triphosphate splitting and polymerization. *J. Mol. Biol.* 44:319–332.
9. Yanagida, T., M. Nakase, K. Nishiyama, and F. Oosawa. 1984. Direct observation of motion of single F-actin filaments in the presence of myosin. *Nature.* 307:58–60.

10. Honda, H., H. Nagashima, and S. Asakura. 1986. Directional movement of F-actin in vitro. *J. Mol. Biol.* 191:131–133.

11. Amann, K. J., and T. D. Pollard. 2001. Direct real-time observation of actin filament branching mediated by Arp2/3 complex using total internal reflection fluorescence microscopy. *Proc. Natl. Acad. Sci. USA.* 98:15009–15013.

12. Fujiwara, I., S. Suetsugu, S. Uemura, T. Takenawa, and S. Ishiwata. 2002. Visualization and force measurement of branching by Arp2/3 complex and N-WASP in actin filament. *Biochem. Biophys. Res. Commun.* 293:1550–1555.

13. Fujiwara, I., S. Takahashi, H. Tadakuma, T. Funatsu, and S. Ishiwata. 2002. Microscopic analysis of polymerization dynamics with individual actin filaments. *Nat. Cell Biol.* 4:666–673.

14. Kuhn, J. R., and T. D. Pollard. 2005. Real-time measurements of actin filament polymerization by total internal reflection fluorescence microscopy. *Biophys. J.* 88:1387–1402.

15. Burlacu, S., P. A. Janmey, and J. Borejdo. 1992. Distribution of actin filament lengths measured by fluorescence microscopy. *Am. J. Physiol.* 262:C569–C577.

16. Oosawa, F., and M. Kasai. 1962. A theory of linear and helical aggregations of macromolecules. *J. Mol. Biol.* 4:10–21.

17. Chen, Y., J. D. Muller, P. T. So, and E. Gratton. 1999. The photon counting histogram in fluorescence fluctuation spectroscopy. *Biophys. J.* 77:553–567.

18. Chen, Y., L. N. Wei, and J. D. Muller. 2003. Probing protein oligomerization in living cells with fluorescence fluctuation spectroscopy. *Proc. Natl. Acad. Sci. USA.* 100:15492–15497.

19. Van Rompaey, E., Y. Chen, J. D. Muller, E. Gratton, E. Van Craenenbroeck, Y. Engelborghs, S. De Smedt, and J. Demeester. 2001. Fluorescence fluctuation analysis for the study of interactions between oligonucleotides and polycationic polymers. *Biol. Chem.* 382:379–386.

20. Huang, B., T. D. Perroud, and R. N. Zare. 2004. Photon counting histogram: one-photon excitation. *ChemPhysChem.* 5:1523–1531.

21. Perroud, T. D., B. Huang, M. I. Wallace, and R. N. Zare. 2003. Photon counting histogram for one-photon excitation. *ChemPhysChem.* 4: 1121–1123.

22. Perroud, T. D., M. P. Bokoch, and R. N. Zare. 2005. Cytochrome *c* conformations resolved by the photon counting histogram: watching the alkaline transition with single-molecule sensitivity. *Proc. Natl. Acad. Sci. USA.* 102:17570–17575.

23. Spudich, J. A., and S. Watt. 1971. The regulation of rabbit skeletal muscle contraction. I. Biochemical studies of the interaction of the tropomyosin-troponin complex with actin and the proteolytic fragments of myosin. *J. Biol. Chem.* 246:4866–4871.

24. Houk, T. W., Jr., and K. Ue. 1974. The measurement of actin concentration in solution: a comparison of methods. *Anal. Biochem.* 62:66–74.

25. Press, W. H., S. A. Teukolsky, W. T. Vetterling, and B. P. Flannery. 1988. Numerical Recipes in C. Cambridge University Press, Cambridge, U.K.